Stick–slip motion in the atomic force microscope

K.L. Johnson and J. Woodhouse

Cambridge University Engineering Department, Trumpington Street, Cambridge CB2 1PZ, UK
E-mail: {klj1000, jw12}@eng.cam.ac.uk

Received 13 March 1998; accepted 20 May 1998

Measurements of atomic friction in the atomic force microscope frequently show periodic variations at the lattice spacing of the surface being scanned, which have the saw-tooth wave form characteristic of "stick–slip" motion. Simple models of this behaviour have been proposed, in which the "dynamic element" of the system is provided by the elastic stiffness and inertia of the cantilever which supports the tip of the microscope, in its lateral, i.e., torsional mode of vibration. These models have been successful in predicting the observed motion, but only by assuming that the cantilever is heavily damped. However, the source of this damping in a highly elastic cantilever is not explained. To resolve the paradox, it is shown in this note that it is necessary to introduce the elastic stiffness of the contact into the model. The relationship between the contact stiffness, the cantilever stiffness and the amplitude of the periodic friction force is derived in order for stick–slip motion at lattice spacing to be achieved.

Keywords: nano-tribology, atomic friction, atomic force microscopy

Measurements of atomic friction in the atomic force microscope frequently, but not universally, show periodic variations at the lattice spacing of the surface being scanned, which have the saw-tooth wave form characteristic of "stick–slip" motion, e.g., Erlandsson et al. [1], Fujisawa et al. [2]. This process has been modelled in a simple way for a one-dimensional scan by Tomanek et al. [3] and for a two-dimensional scan by Holscher et al. [4], with considerable success in reproducing the observed variations in friction force, notably in the two-dimensional case where the microscope tip responds to motion and forces in both longitudinal and lateral directions.

Despite this success, these models incorporate idealisations which raise questions on physical grounds:

(1) Friction is measured by the torsional deflexion of the elastic cantilever which supports the contacting tip. The above models recognise that the compliance and inertia of the cantilever comprise a dynamical system which responds to the fluctuation in friction force. Following an unstable jump ("slip"), the cantilever carrying the tip oscillates in its torsional mode. In the models referred to above it has been assumed that such vibrations are heavily damped. In the absence of this assumption the models do not predict regular stick–slip motion at lattice spacing as generally observed: instead "multiple jumps" and irregular motion are predicted. However, the cantilever is highly elastic and so would be expected to have low inherent damping. This paradox will be examined.

(2) More recently, however, it has been recognised that an additional compliance is provided between the end of the cantilever and the specimen by the contact of the tip and specimen. This is the tangential analogue of the normal compliance of a Hertz contact (see Johnson [5, pp. 216–220]). It has been measured by Lantz et al. [6] and by Carpick et al. [7]. The effect of this additional compliance on the dynamics of the system will be considered in this note.

(3) The contact area of a typical AFM tip in a friction test has a radius of around 4 nm, which corresponds to around 100 atoms. The models mentioned above assume a sinusoidal interaction potential varying at the lattice spacing of the specimen. This is an obvious concept with a tip comprising a single atom, but how the atoms actually move during sliding of a tip of finite contact size and their influence on the interaction potential is an open question which will not be pursued here.

Since the limited aim of this investigation was to examine the influence of the contact compliance on the dynamics of the system and, if possible, to resolve the paradox concerning damping, it was decided to adopt the idealisations in the earlier models in all other respects. Further, since these issues apply equally to one- and two-dimensional motion, a one-dimensional line scan was considered for simplicity.

The cantilever and tip in its lateral (torsional) mode is shown in figure 1(a); the equivalent spring-mass system is shown in figure 1(b). The lateral displacement of the tip due to twist θ is denoted by x and that due to tangential compliance of the contact by z. The cantilever lateral stiffness is $k_l = T_l/x$ and the combined stiffness of the tip and contact is $k_c = T_c/z$, where T_l and T_c are the tensions in the two springs shown in figure 1(b). The mass m is the equivalent mass of the cantilever associated with its fundamental torsional frequency $\omega_l = \sqrt{k_l/m}$. Motion in the higher modes is likely to be small and will be neglected.

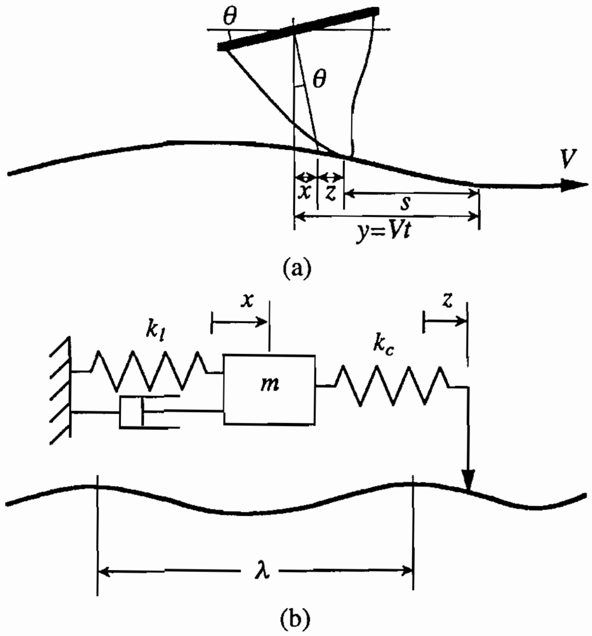

Figure 1. (a) AFM cantilever in lateral mode. Torsional displacement of the cantilever θ gives lateral displacement x; z = contact displacement; s = slip. (b) Equivalent dynamical system, where k_l and m represent the stiffness and inertia of the cantilever and k_c represents the contact stiffness.

The total static compliance c of the system is then given by

$$c = 1/k_e = 1/k_l + 1/k_c. \tag{1}$$

Following Tomanek et al. [3] a force potential is assumed which gives rise to a sinusoidal variation of tangential force at the lattice spacing λ of the specimen surface, expressed by

$$T_c(s) = T^* \sin(2\pi s/\lambda), \tag{2}$$

where s is the tangential displacement (slip) of the specimen relative to the tip. Assuming that the cantilever is damped by a viscous force b, its motion is given by

$$m\left(\frac{\mathrm{d}^2x}{\mathrm{d}t^2}\right)+b\left(\frac{\mathrm{d}x}{\mathrm{d}t}\right) = T_c - T_l = T^*\sin(2\pi s/\lambda) - k_l x. \tag{3}$$

During a scan the surface is displaced by $y(t) = Vt$, where V is the scan velocity. The slip may then be expressed by

$$s = y - x - z = y - x - (1/k_c)T^*\sin(2\pi s/\lambda). \tag{4}$$

Under quasi-static conditions $(\mathrm{d}^2x/\mathrm{d}t^2) = 0$, so that

$$s = Vt - T_c\{1/k_c + 1/k_l\} = Vt - T_c/k_e. \tag{5}$$

We now introduce the non-dimensional notation:

$$S = s/\lambda, \quad X = x/\lambda, \quad Y = y/\lambda, \quad Z = z/\lambda,$$

$$F_c = T_c/T^*, \quad F_l = T_l/T^*,$$

$$K_c = \lambda k_c/T^*, \quad K_l = \lambda k_l/T^*,$$

$$q = \omega_l t, \quad \delta = b\omega_l/2k_l,$$

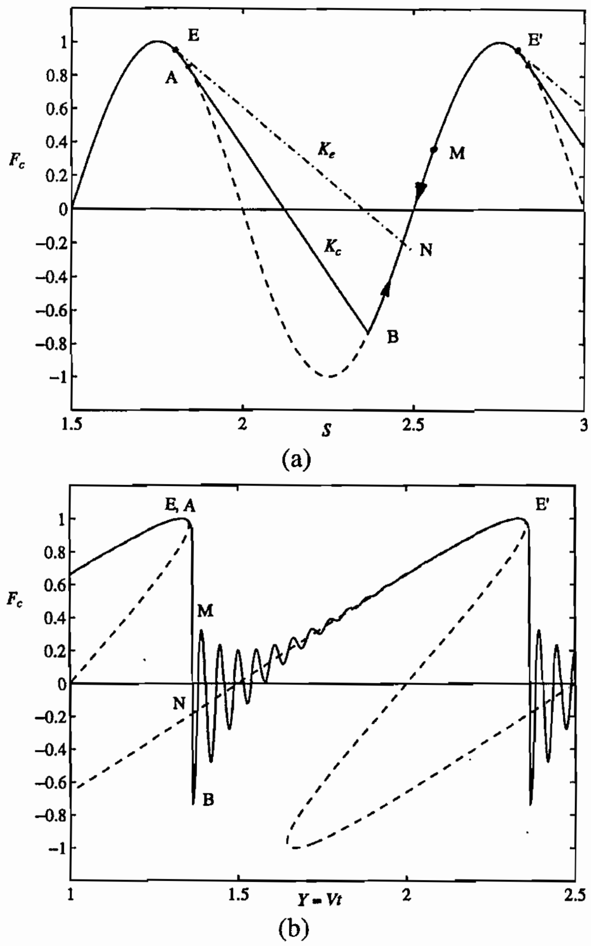

Figure 2. (a) Sinusoidal variation of friction force F_c. The contact spring becomes unstable at A and snaps through to B. The cantilever becomes unstable at E, and oscillates about an equilibrium position starting at N, with a maximum overshoot to M. (b) Contact force to a base of scan displacement Y, showing the "saw-tooth" wave form associated with stick–slip.

where $\omega_l = \sqrt{k_l/m}$ as above. In terms of these variables equations (3)–(5) may be written:

$$F_c = \sin(2\pi S) = K_l\left\{\frac{\mathrm{d}^2X}{\mathrm{d}q^2} + 2\delta\frac{\mathrm{d}X}{\mathrm{d}q} + X\right\}, \tag{6}$$

$$S = Y - X - (1/K_c)\sin(2\pi S), \tag{7}$$

and under quasi-static conditions

$$S = Y - F_c/K_e = Y - (1/K_e)\sin(2\pi S). \tag{8}$$

The simultaneous solution of equations (6) and (7) must be obtained numerically. An efficient algorithm for this process is given in appendix A. As an illustrative example, the solution for $K_l = 4$, $K_c = 3$, $\delta = 0.1$ and $2\pi V/\lambda\omega_l = 15$ is presented in figure 2.

In the absence of dynamic effects, equation (8) applies. Its solution is given in figure 2(a) by the intersection of $F_c(S)$ by a line of slope $-K_e$ which, during a scan, traverses to the right with the scan velocity V.

Starting from an intersection point at O, where $F_c = F_l = S = X = Z = Vt/\lambda = 0$, intersection points in the segment OE are stable and quasi-static. The tangent point E locates the onset of instability at which the cantilever starts to move according to equation (6) at a rate governed by the combined stiffness K_e. At point A, at which the slope of $F_c(S)$ is $-K_c$, the contact "spring" becomes unstable and snaps through to point B. Since the contact spring has negligible mass, it will relax in a time of the order of that for a stress wave to traverse the contact diameter, of order 10^{-12} s, which is short compared with the natural period of the cantilever. Thus, at B, $X_B = X_A$ and $[dX/dt]_B = [dX/dt]_A \approx 0$. The strain energy released in this relaxation will be entirely dissipated in phonons. Subsequently the extension of the contact spring Z will be quasi-static and given by $F_c(S)/K_c$. The dynamical behaviour of such an elastic contact is discussed in [5, pp. 343–349].

The subsequent motion is one of damped oscillation of the cantilever at its natural frequency ω_l. In figure 2(a) the friction force F_c fluctuates in the segment BM until it damps out and a second cycle begins. In figure 2(b) the friction force is plotted against the scanning displacement Y, showing the snap-through from A to B, followed by the cantilever oscillation. For the purpose of illustration of the motion, an untypically low value of the cantilever frequency ω_l and high value of the damping factor δ have been used in the calculation of figure 2. In reality, the period of the oscillation will be much shorter than shown. Even if the damping factor is much less than 0.1, the oscillation will have died out before the next point of instability E′ is reached. In any case, the recording equipment of the AFM is unlikely to resolve the oscillatory motion, whereupon the familiar saw-tooth wave form associated with stick–slip will be observed. We note that the overshoot $[(F_c)_M - (F_c)_N]$ is approximately equal to $[(F_c)_N - (F_c)_B]$.

In the example shown in figure 2 the stick–slip motion takes place at the lattice spacing λ of the specimen. A cantilever of lower stiffness, however, would reduce the combined stiffness K_e, which would raise the point N in the figure and hence the height of the first overshoot M. If the overshoot reaches the instability point E′ in the next cycle, the cantilever will jump (slip) two or possibly more cycles before sticking. In the numerical solution of equations (6) and (7), M is located by the first occasion when $dS/dq = 0$. Denoting the maximum value of S in the first overshoot by S_M, multiple jumps will be avoided if $S_M < S_{E'}$. In this calculation the "worst case" is obtained by taking the damping δ in the cantilever to be zero. Also, since the frequency of the cantilever is much higher than the lattice scan frequency, the scanning displacement $(Y_M - Y_E)$ during the slip from E to M is neglected. The results of these calculations are shown in figure 3, which specifies the threshold of multiple jumps.

Energy is dissipated in the snap-through from A to B. However, if the contact stiffness k_c exceeds the maximum gradient of $T_c(s)$, i.e., if $K_c > 2\pi$, the contact "spring" will be continuously stable and no snap through will occur. In these circumstances, neglecting cantilever damping, energy of the system will be conserved between E and E′. It is shown in appendix B that, at the threshold of multiple jumps, the cantilever and contact stiffnesses K_l and K_c are related by the equation

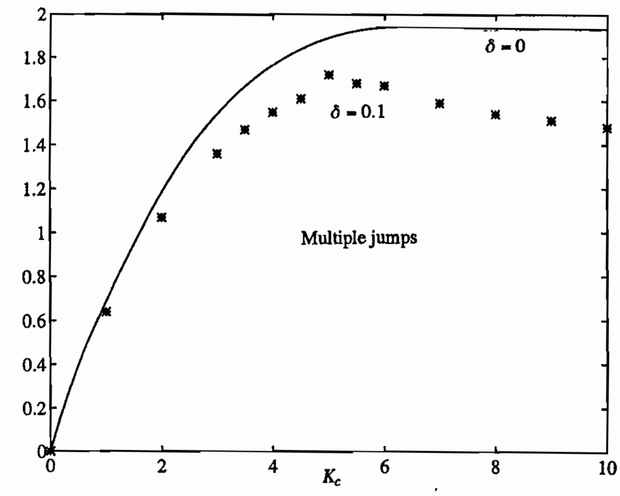

Figure 3. Map of cantilever and contact stiffnesses, K_l and K_c, showing the threshold of multiple jumps: (i) neglecting cantilever damping ($\delta = 0$); (ii) $\delta = 0.1$.

$$(K_l/2)^2 + (K_e/2\pi)^2 = 1.0, \tag{9}$$

where K_e can be expressed in terms of K_l and K_c by equation (1). When the contact stiffness is small ($\ll 2\pi$), multiple jumps will not occur if $K_l > 0.75K_c$.

The effect of damping in the cantilever is to reduce the height of the overshoot and hence to reduce the likelihood of multiple jumps. Some individual computed points using a cantilever damping factor $\delta = 0.1$ are shown in figure 3.

To illustrate the occurrence of multiple jumps two cases have been computed, one on each side of the threshold ($\delta = 0.1$) in figure 3. In the first (figure 4(a)) $K_c = 3$ and $K_l = 1.4$, which lies just above the threshold, so that a slip occurs at each lattice spacing ($Vt/\lambda = 1$). The first overshoot very nearly reaches the limit before decaying. In the second example (figure 4(b)) $K_c = 3$ and $K_l = 1.3$, which lies just below the threshold. The first overshoot (which can be just detected in the figure) carries the slip into the next lattice spacing before decaying into the stick phase, which occupies a period $Vt/\lambda = 2$. If the cantilever stiffness is further reduced it is possible to slip three or more spacings before sticking.

Finally we note that the motion is steady, without stick–slip, if the combined stiffness k_e exceeds the maximum gradient of $T_c(s)$, i.e., if $K_e = K_cK_l/(K_c + K_l) > 2\pi$. Even so the graph of force (F_c) against displacement (Y) may still be very unsymmetrical. We note that this condition of steady motion may be realised, even with compliant springs, if the amplitude T^* of the periodic force is sufficiently small.

Energy dissipated by phonons in the snap-through of the contact and in the damping of oscillations of the cantilever contribute to sliding friction. The mean friction force may

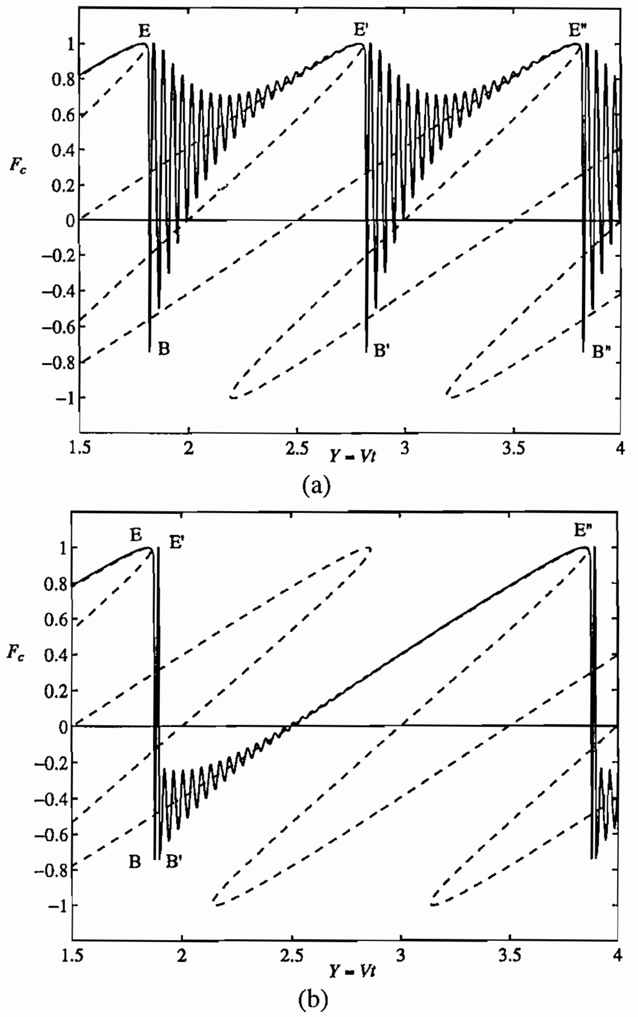

Figure 4. Motion close to the threshold ($\delta = 0.1$) shown in figure 3. (a) $K_c = 3$, $K_l = 1.4$. This point lies just above the threshold so that the first overshoot does not quite reach E′ and the motion is periodic at the lattice spacing. (b) $K_c = 3$, $K_l = 1.3$. This point lies just below the threshold. The first overshoot carries the motion beyond E′ into the next spacing, giving rise to periodicity at twice the lattice spacing.

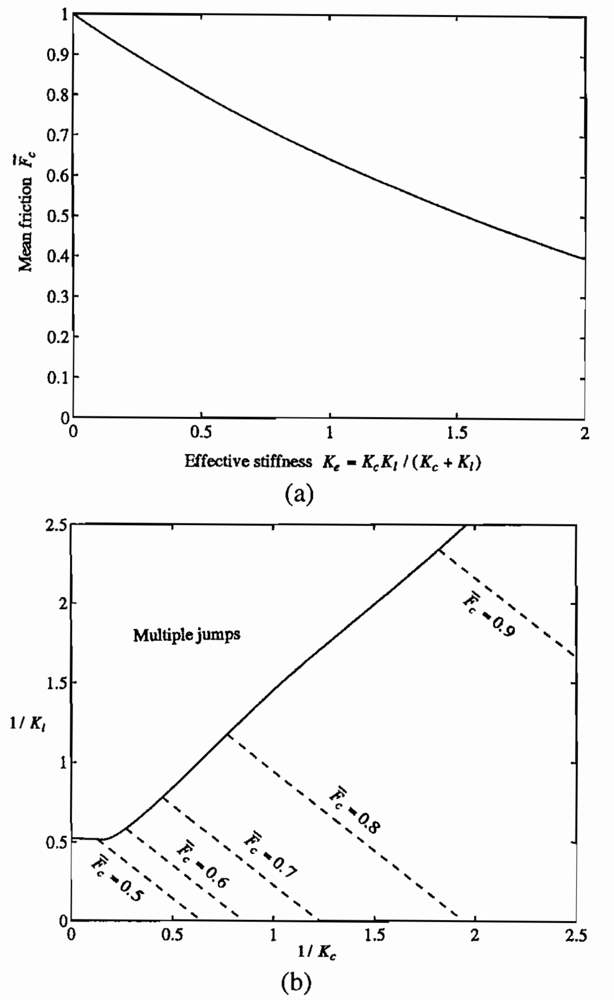

Figure 5. The influence of cantilever and contact stiffnesses on the mean friction force. (a) Calculated from equation (10). (b) Mean friction contours in terms of K_l and K_c.

be calculated from the stable part of the force-displacement curve, thus

$$T = \frac{1}{\lambda}\int_{S_{\mathrm{N}}}^{S_{\mathrm{E}}} T\,\mathrm{d}y,$$

i.e.,

$$\begin{aligned}\overline{F}_c &= \int_{S_{\mathrm{N}}}^{S_{\mathrm{E}}} F_c\,\mathrm{d}Y = \int_{S_{\mathrm{N}}}^{S_{\mathrm{E}}} \sin(2\pi S)\left[1 + \frac{2\pi}{K_e}\cos(2\pi S)\right]\mathrm{d}S \\ &= -\frac{1}{2\pi}\big[\cos(2\pi S)\big]_{S_{\mathrm{N}}}^{S_{\mathrm{E}}} - \frac{1}{4K_e}\big[\cos(4\pi S)\big]_{S_{\mathrm{N}}}^{S_{\mathrm{E}}}. \qquad (10)\end{aligned}$$

Computations of $\overline{F}_c$ are shown as a function of K_e in figure 5(a). The mean friction varies from zero when the entire cycle is stable ($K_e > 2\pi$), and approaches 1.0 (i.e., $T \to T^*$) when $K_e \to 0$. Similar calculations have been made by Colchero et al. [8]. The results in figure 5(a) have been used, together with the data of figure 3, to produce the map in figure 5(b), which shows contours of non-dimensional friction $\overline{F}_c(=\overline{T}_c/T^*)$ in terms of the compliances $1/K_c$ and $1/K_l$.

Conclusions

(1) It is generally realised that the existence of stick–slip motion in the atomic friction microscope depends upon the lateral compliance of the measuring system (cantilever and tip) in relation to the amplitude of the lateral force potential. In this note the compliance of the tip and contact region has been separated from that of the force-measuring cantilever in a simplified study of the dynamic response of the system. A significant feature of the behaviour lies in their very different frequencies of response. The lattice traverse frequency: ≈ 100 Hz; the cantilever frequency: $\approx 10^5$ Hz; the tip and contact frequency: $\approx 10^{12}$ Hz.

(2) The instability inherent in stick–slip motion excites vibrations of the cantilever at its natural frequency which, for a sufficiently compliant cantilever, could cause a jump of more than one lattice spacing in each "slip".

It is shown in this note that the slip of the tip and contact spring is purely dissipative, which helps to damp the motion of the cantilever and to reduce the likelihood of multiple jumps. It is shown that multiple jumps are avoided: when the non-dimensional contact stiffness $K_c > 2\pi$, if the cantilever stiffness $K_l > 1.9$, and under all circumstances if $K_l > 0.75K_c$.

In the experiments of Carpick et al. [7] the cantilever stiffness k_l was estimated to be 190 N/m, while the combined stiffness of tip and contact k_c varied with load from 9.5 to 66 N/m. In the experiments of Lantz et al. [6], the cantilever stiffness $k_l = 110$ N/m. The stiffnesses of the tip itself and the contact deformation were estimated separately to vary from 84 to 108 N/m and 60 to 100 N/m respectively, giving the variation of the combined tip and contact stiffness $k_c = 35$–52 N/m. We note that throughout the range of both sets of experiments $k_l > k_c$, whereby $K_l > K_c$, so that multiple jumps would not be expected. Carpick et al. observed stick–slip at single lattice spacing as predicted. Lantz et al. did not record any stick–slip motion, which would imply that the amplitude of the periodic tangential force was too small in relation to the equivalent stiffness k_e, i.e., $T^* < \lambda K_e/2\pi$.

It would appear from this limited data that the relative cantilever and contact stiffnesses in typical AFM applications are such as to eliminate multiple slips. It would be instructive, however, to carry out an experiment with a very compliant cantilever to see whether the multiple slips predicted by this model actually occur.

(3) Stick–slip motion implies frictional energy dissipation, such that the mean level of the friction trace, as shown in figure 2(b), lies above zero. As the effective stiffness k_e is reduced, the mean friction increases and the drop at slip decreases. However, the mean friction observed in the experiments of Erlandsson et al. and Carpick et al., for example, show a mean friction which is higher than would be expected by this mechanism alone. It would appear that the tangential force has a steady component in addition to the sinusoidally fluctuating component considered in this note. As mentioned above, the combination of steady and fluctuating components presumably arises from the finite size of the contact area and the probable irregularity of the atomic structure of the tip. This aspect of the problem presents a challenge for atomic modelling.

(4) It is recognised that a sinusoidal potential provides only the simplest representation of a periodic friction force, and that the threshold of multiple slips presented in figure 3 is likely to be influenced to some extent by the form of the potential. Work is in progress to examine the behaviour of a contact consisting of many atoms and its influence on the frictional potential.

Acknowledgement

The authors wish to thank the following for stimulating discussion of an earlier draft: N. Burnham, J. Colchero, H. Hoelscher, G. McClelland, U.D. Schwarz and M.E. Welland.

Appendix A

To produce the numerical simulations shown in figures 2(b) and 4, an efficient algorithm was employed which has been used in the past for simulation of nonlinear oscillations of musical instruments (including real-time simulation for musical synthesis): see McIntyre et al. [9]. Writing the solution of equation (6) in terms of its Green's function, the problem is to solve simultaneously

$$K_c Z = \sin 2\pi(Vt/\lambda - X - Z) \tag{A1}$$

and

$$\begin{aligned} X(t) &= \frac{K_c\omega}{K_l}\int_0^t \sin\omega(t-\tau)\exp[-\delta(t-\tau)]Z(\tau)\,\mathrm{d}\tau \\ &= \mathrm{Im}\left\{\frac{K_c\omega}{K_l}\int_0^t \exp[(\mathrm{i}\omega-\delta)(t-\tau)]Z(\tau)\,\mathrm{d}\tau\right\}. \end{aligned} \tag{A2}$$

For a short time step h, (A2) can readily be shown to imply

$$\overline{X}(t+h) \approx \frac{K_c\omega}{K_l}Z(t)h + \mathrm{e}^{(\mathrm{i}\omega-\delta)}\overline{X}(t), \tag{A3}$$

where

$$X(t) = \mathrm{Im}\{\overline{X}(t)\}.$$

Thus for each time step, the apparently time consuming convolution integral can be evaluated with a single complex multiplication and addition to yield the new value of $X(t)$. The new value of $Z(t)$ is then found from (A1), by linear extrapolation from the previous value, improved if necessary by a few Newton–Raphson iterations. If jumps are present, these must be detected and implemented at this stage.

Appendix B

In this appendix the threshold of multiple jumps is investigated for the case in which the contact spring is stable throughout, i.e., when $K_c > 2\pi$. Thus no energy is dissipated at the contact and, in the "worst case", damping in the cantilever is taken to be zero, so that total energy is conserved throughout the motion. At the threshold the velocity of the cantilever will fall to zero at the instability points E and E′ etc. in figure 2(a). In a complete cycle from E to E′ the work done by the sinusoidal fricton force F_c is zero, so that the elastic strain energy in the cantilever is conserved as it swings from maximum tension at E to maximum compression at E′, through a total displacement:

$$X_{\mathrm{E}'} - X_{\mathrm{E}} = S_{\mathrm{E}'} - S_{\mathrm{E}} = 1.0$$

and

$$(F_l)_{E'} = -(F_l)_E = -(F_c)_E = -\sin(2\pi S_E),$$

hence

$$(2/K_l)\sin(2\pi S_E) = 1.0. \qquad (A4)$$

Now E is the point where the gradient of $T_c(S)$ equals the combined stiffness, i.e.,

$$2\pi\cos(2\pi S_E) = -K_e, \qquad (A5)$$

which give

$$(K_l/2)^2 + (K_e/2\pi)^2 = \sin^2(2\pi S_E) + \cos^2(2\pi S_E) = 1.0. \qquad (A6)$$

Recalling that $K_e = K_l K_c/(K_l + K_c)$, this equation relates the cantilever and contact stiffnesses K_l and K_c at the threshold of multiple jumps when $K_c > 2\pi$.

References

[1] R. Erlandsson, G. Hadziioannou, C.M. Mate, G.M. McLelland and S. Chiang, J. Chem. Phys. 89 (1988) 5190.
[2] S. Fujisawa, E. Kishi, Y. Sugawara and S. Morita, Nanotechnology 5 (1994) 8.
[3] D. Tomanek, W. Zhong and H. Thomas, Europhys. Lett. 15 (1991) 887.
[4] H. Holscher, U.D. Schwartz and R. Wiesendanger, in: *Micro/Nano-tribology and its Applications*, ed. B. Bushan (Kluwer, Dordrecht, 1997).
[5] K.L. Johnson, *Contact Mechanics* (Cambridge University Press, Cambridge, 1985).
[6] M.A. Lantz, S.J. O'Shea, M.E. Welland and K.L. Johnson, Phys. Rev. B 55 (1997) 10776.
[7] R.W. Carpick, D.F. Ogletree and M. Salmeron, Appl. Phys. Lett. 70 (1997) 1.
[8] J. Colchero, A.M. Baro and O. Marti, Tribology Lett. 2 (1996) 327.
[9] M.E. McIntyre, R.T. Schumacher and J. Woodhouse, J. Acoust. Soc. Am. 74 (1983) 1325.